Electronic Supplementary Material (ESI) for Materials Horizons.

Supplementary Information

High-Performance Y5-SWCNT Thermoelectric Alloy Produced by Pre-Crystallization Filtration

Peiyao Liu,‡ [a] Hongbin Sun,‡ [a] Xin Wu, [a] Hanlin Wang, [b] Qiang Zhao, [c] Zhenjie Ni*[a,d] and Cun-Yue Guo*[a]

[a] School of Chemical Sciences, University of Chinese Academy of Sciences, Beijing 101408, China.

[b] Beijing National Laboratory for Molecular Sciences, Key Laboratory of Organic Solids, Institute of Chemistry, Chinese Academy of Sciences, Beijing 100190, China.

[c] College of Science, Civil Aviation University of China, Tianjin 300300, China.

[d] Binzhou Institute of Technology, Binzhou 256606, China.

‡ These authors contribute equally to this work.

Corresponding Author

* Zhenjie Ni: nizhenjie@ucas.ac.cn;

* Cun-Yue Guo: cyguo@ucas.ac.cn

Table S1 Comparison of thermoelectric performance of organic small molecules (OSMs)/single-walled carbon nanotubes (SWCNTs)-based thin films.

Materials	σ (S cm^{-1})	S (μV K^{-1})	PF (μW m^{-1} K^{-2})	Ref.
MGH (BenzOH)/SWCNT	588	58	200	1
ADTAg/SWCNT	924.1 ± 45.3	47.8 ± 3.9	211.6 ± 9.9	2
C8C12-NDI/SWCNT	515.6	55.49	158.8	3
ZnTPP/SWCNT	926.7 ± 24.8	46.9	203.8 ± 32.9	4
PhC_2Cu/SWCNT	666.2 ± 6.7	~ 55	200.2 ± 10.9	5
HAT6/SWCNT	979.32 ± 31.84	48.02 ± 0.43	225.77 ± 2.66	6
PyBOP/SWCNT	3731.5 ± 183.5	21.6 ± 0.9	174.0 ± 1.7	7
CzS/SWCNT	264.0 ± 28.0	106.5 ± 2.3	299.8 ± 37.4	8
SM-Ph-2F/SWCNT	1001.8 ± 166.4	46.5 ± 5.2	214.0 ± 25.8	9
PCF-Y5(5%)/SWCNT	818.91 ± 47.51	54.33 ± 0.75	241.93 ± 19.06	**This work**

Table S2 Comparison of thermoelectric performance of PCF-Y5/SWCNT and polymer/carbon nanotube composites.

Materials	σ (S cm^{-1})	S (μV K^{-1})	PF (μW m^{-1} K^{-2})	Ref.
PANI/50 wt% SWCNT	331.25 ± 8.49	47.06	73.33 ± 2.03	10
P(NDI-HTO)/ 90 wt% p-SWCNT	1184.0 ± 131.8	-	264.1 ± 21.9	11
PEDOT:PSS/SWNCT	1562 ± 170	21.8 ± 0.5	73.9 ± 4.7	12
P3HT/60 wt% SWCNT	~716	~48.61	169.2 ± 13.5	13
PE/PEDOT/72 wt% SWCNT	~459.8	47.58	103.81	14
PCF-Y5(5%)/SWCNT	818.91 ± 47.51	54.33 ± 0.75	241.93 ± 19.06	**This work**

General Considerations

The starting materials and additives were obtained commercially and used directly. $CHCl_3$ (AR, ≥ 99%) was purchased from Beijing Tongguang Fine Chemical Company. MeOH (AR, ≥ 99.5 %) and DCM (AR, ≥ 99.5 %) were provided by Shanghai Titan Scientific Col., Ltd. Pyridine (AR, ≥ 99.5 %) was bought from Anneji (Shanghai) Pharmaceutical Chemical Co., Ltd. Y6-CHO was purchased from Zhengzhou Alfa Chemical Co., Ltd. IC, IC-2F, and IC-2Cl were purchased from Shanghai Haohong Scientific Co., Ltd. The reactive ball-milling is carried out with Grinding jar used Retsch MM400 mill. Both jars (1.5 mL) and balls (5 mm) are made of stainless (SUS400B and SUS420J2, respectively). SWCNTs (diameter: 1−2 nm, purity: > 95.0%) were purchased from Jiangsu XFNANO Co. Ltd, China. Ultrasonic cell disruptor was purchased from Beijing Xinying Weiye Technology Co., Ltd, China. The silica gel was purchased from Qingdao Ocean Chemicals. Analytical Thin Layer Chromatography (TLC) was visualized with a UV lamp at 254 nm and 365 nm and was purchased from Yantai Yinlong. NMR spectra were recorded on a JEOL 400, JEOL 600 spectrometer. ^{1}H and ^{13}C chemical shifts are reported in parts per million (ppm) relative to trimethylsilane (TMS), with the residual solvent peak used as an internal reference. Proton (^{1}H) NMR information is given in the following format: multiplicity (s, singlet; d, doublet; t, triplet; q, quartet; qui, quintet; sept, septet; m, multiplet), coupling constant (*J*) in Hertz (Hz), number of protons. The morphology of these composites was observed by High Resolution Field Emission Scanning Electron Microscope (SEM, SU8010) and Transmission electron microscope (TEM, HT-7700Exalens, Japan). The elemental analysis of the film is performed by the area scanning of energy dispersive spectroscopy (EDS, SU8010). With an excitation wavelength of 532 nm, the Raman spectra are performed using a Raman spectrometer (Renishaw in Via Reflex). The binding energy are measured by X-ray photoelectron

spectroscopy (XPS, AXIS Supra by Kratos Analytical with an Al Kα X-ray source (1486.8 eV)) and the work functions are calculated by ultraviolet photoelectron spectroscopy (UPS, AXIS Supra). The electrical conductivity (σ) and the Seebeck coefficient (S)of the composite films are measured by a TE parameter test system (MRS-3, JiaYiTong Company).

Preparation of n-type PEI/SWCNT composite film

Add 10 mg of SWCNTs and 500 mg of PEI into a beaker, then add 25 mL of methanol. Using an ultrasonic cell disruptor, sonicate the mixture for 1 h in an ice water bath. The mixture was filtered by a nylon membrane with a pore size of 0.2 μm under vacuum to obtain the composite material, and finally dried at 65 °C for 3 h to completely remove the solvent, resulting in PEI/SWCNT composite films.

Synthesis by ball milling

The last step of the synthesis of Y5, Y6, and Y7 requires the classical Knoevenagel condensation reaction to connect aldehyde-terminated aromatic fused-ring and the activated methylene-based end-capping group , but the traditional Knoevenagel condensation reaction be carried out in a halogen-containing solvent with high toxicity, low yield and many by-products, which makes the high cost and goes against the concept of energy green environment[15]. In this paper, small molecules were prepared by ball milling. Ball milling is a mechanochemical method that allows the reaction to be performed quantitatively and quickly without solvents or with trace additives. Compared with the traditional synthesis method, it has the advantages of high reaction selectivity, green environmental protection and can greatly reduce the reaction time[16-20].

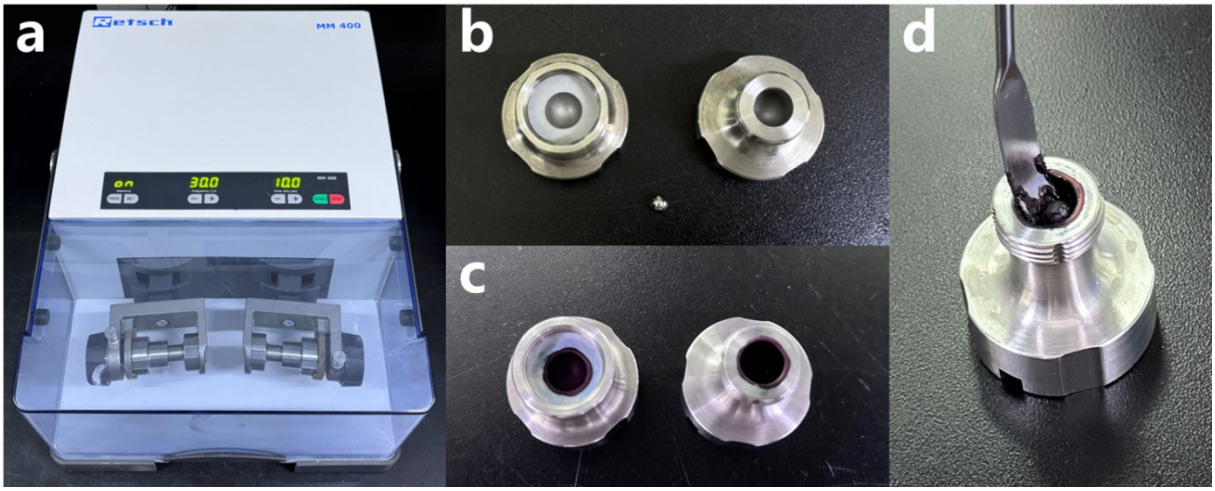

Fig. S1. a Retsch MM400 used in synthesis; **b** Stainless jar and ball used in synthesis; **c** The state at the end of the reaction; **d** The shape of the final product.

Synthesis of Y5. (2,2′-((2Z,2′Z)-((12,13-bis(2-ethylhexyl)-3,9-diundecyl-12,13-dihydro[1,2,5]thiadiazolo[3,4-e]thieno[2″,3″:4′,5′]thieno[2′,3′:4,5]pyrrolo[3,2-g]thieno[2′,3′:4,5]thieno[3,2-*b*]indole-2,10-diyl)bis(methanylylidene))bis(3-oxo-2,3-dihydro1H-indene-2,1-diylidene))dimalononitrile)

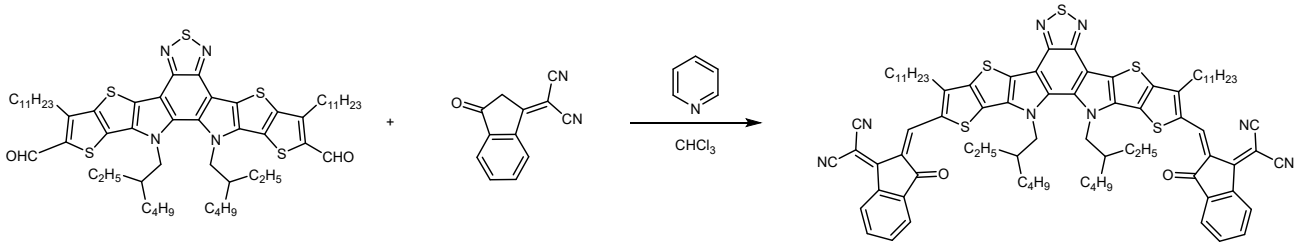

Scheme 1. Synthetic routes of **Y5**.

Y6-CHO (52 mg, 0.05 mmol) and **IC** (20 mg, 0.1 mmol) were placed in a ball milling vessel with a grinding ball, then the DCM (50 μL) and pyridine (0.5 mmol) were added with a pipette gun. After that, the vessel was placed in the ball mill (Retsch MM400 mill, 30 Hz). After 45 min to 3 h, the mixture was dissolved with DCM, and the crude product was distilled under reduced pressure. The

crude product was purified by silica gel column chromatography with DCM/PE eluent and recrystallized by $CHCl_3$/MeOH to obtain a black solid (68 mg, 98%). **^{1}H NMR** (600 MHz, Chloroform-d) δ 9.12 (s, 2H), 8.72-8.62(m, 2H), 7.99-7.95 (m, 2H), 7.78-7.75 (m, 4H), 4.83-4.74 (m, 4H), 3.25-3.15 (m, 4H), 2.20-2.11 (m, 2H), 1.91-1.82 (m, 4H), 1.49 (p, J = 7.5 Hz, 4H), 1.35 (p, J = 7.6 Hz, 4H), 1.30-1.15 (m, 28H), 1.14-1.05 (m, 12H), 0.85 (t, J = 7.0 Hz, 6H), 0.80-0.74 (m, 6H), 0.70-0.65 (m, 6H).

Synthesis of Y6. (2,2′-((2Z,2′Z)-((12,13-bis(2-ethylhexyl)-3,9-diundecyl-12,13-dihydro-[1,2,5]thiadiazolo[3,4-e]thieno[2″,3″:4′,5′]thieno[2′,3′:4,5]pyrrolo[3,2-g]thieno[2′,3′:4,5]thieno[3,2-*b*]indole-2,10-diyl)bis(methanylylidene))bis(5,6-difluoro-3-oxo-2,3-dihydro-1H-indene-2,1-diylidene))dimalononitrile)

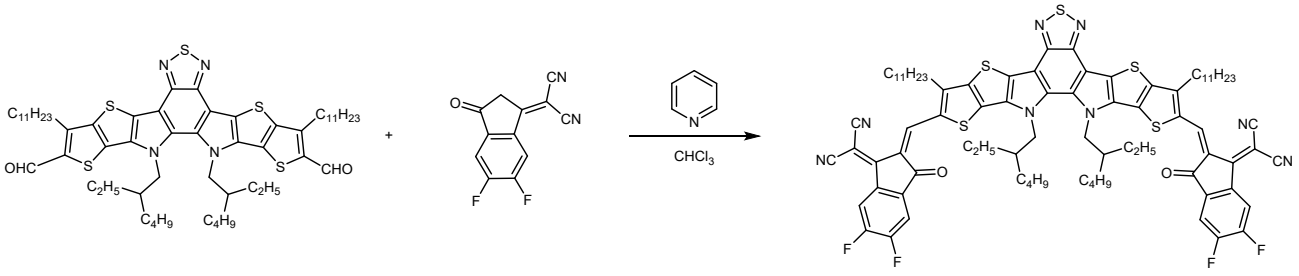

Y6-CHO **IC-2F** **Y6**

Scheme 2. Synthetic routes of **Y6**.

The synthesis step is the same as **Y5**，the reaction initiation substrate was **Y6-CHO** (52 mg, 0.05 mmol) and **IC-2F** (23 mg, 0.1 mmol), the reaction time was 1.5 h, obtain a black solid (65 mg, 90%).**^{1}H NMR** (600 MHz, Chloroform-d) δ 9.16 (s, 2H), 8.53 (dd, J = 9.8, 6.4 Hz, 2H), 7.71 (t, J = 7.3 Hz, 2H), 4.78 (q, J = 14.3, 10.9 Hz, 4H), 3.23-3.15 (m, 4H), 2.16-2.10 (m, 2H), 1.87 (p, J = 7.8 Hz, 4H), 1.50 (p, J = 7.8, 7.4 Hz, 4H), 1.39-1.32 (m, 4H), 1.31-1.18 (m, 28H), 1.14-1.01 (m, 12H), 0.86 (t, J = 7.0 Hz, 6H), 0.79-0.74 (m, 6H), 0.70-0.66 (m, 6H).

Synthesis of Y7. (2,2′-((2Z,2′Z)-((12,13-bis(2-ethylhexyl)-3,9-diundecyl-12,13-dihydro-

[1,2,5]thiadiazolo[3,4-e]thieno[2″,3″:4′,5′]thieno[2′,3′:4,5]pyrrolo[3,2-g]thieno[2′,3′:4,5]thieno[3,2-*b*]indole-2,10-diyl)bis(methanylylidene))bis(5,6-dichloro-3-oxo-2,3-dihydro-1H-indene-2,1-diylidene))dimalononitrile)

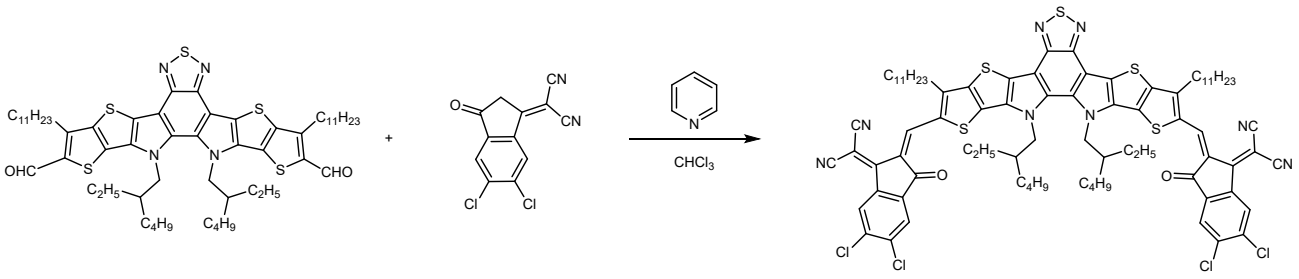

Scheme 3. Synthetic routes of **Y7**.

The synthesis step is the same as **Y5**，the reaction initiation substrate was **Y6-CHO** (52 mg, 0.05 mmol) and **IC-2Cl** (26.3 mg, 0.1 mmol), the reaction time was 3 h, obtain a black solid (41 mg, 54%).**^{1}H NMR** (600 MHz, Chloroform-d) δ 9.16 (s, 2H), 8.78 (s, 2H), 7.97 (s, 2H), 4.81-4.74 (m, 4H), 3.22 (t, J = 8.0 Hz, 4H), 2.10 (p, J = 7.3 Hz, 2H), 1.86 (q, J = 7.9 Hz, 4H), 1.50 (t, J = 7.6 Hz, 4H), 1.38-1.34 (m, 4H), 1.29-1.23 (m, 28H), 1.10-1.00 (m, 12H), 0.89-0.84 (m, 6H), 0.78-0.74 (m, 6H), 0.69-0.65 (m, 6H).

Electronic energy levels of Y5 were studied by cyclic voltammetry

The cyclic voltammetry results were obtained with a computer-controlled Gamry Refence 620 electrochemical workstation using Y5 films on platinum electrode (1.0 cm^2) as the working electrode, a platinum wire as the counter electrode and Ag/AgCl (0.1 M) as the reference electrode in an anhydrous and argon-saturated solution of 0.1 M of tetrabutylammonium hexafluorophosphate (Bu_4NPF_6) in acetonitrile, at a scanning rate of 50 $mV \cdot s^{-1}$. Electrochemical onsets were determined at the position where the current started to rise from the baseline. The highest occupied molecular orbital (HOMO) and lowest occupied molecular orbital (LUMO) levels were calculated by:

$$E_{HOMO} = -(4.8 - 0.47 + E_{onset}^{ox}) \text{ eV}$$

$$E_{LUMO} = -(4.8 - 0.39 + E_{onset}^{red})\ eV$$

The HOMO level is −5.5 eV and the LUMO level is −3.82 eV, which is consistent with the data reported in the literature[21].

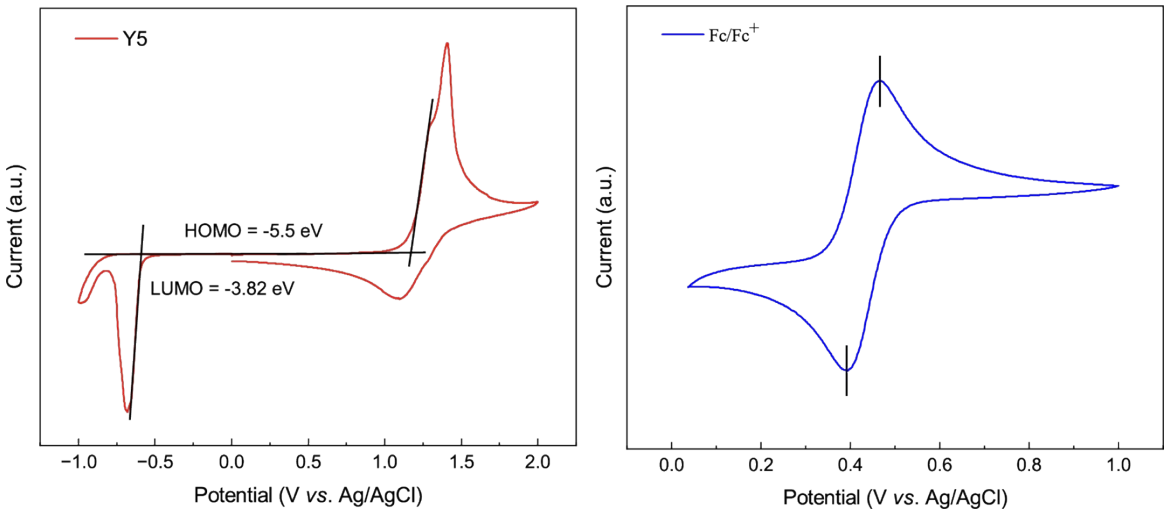

Fig. S2. Cyclic voltammogram of Y5 in acetonitrile solution with 0.1 M Bu_4PF_6 as the supporting electrolyte with a scan speed of 50 mV s^{-1}.

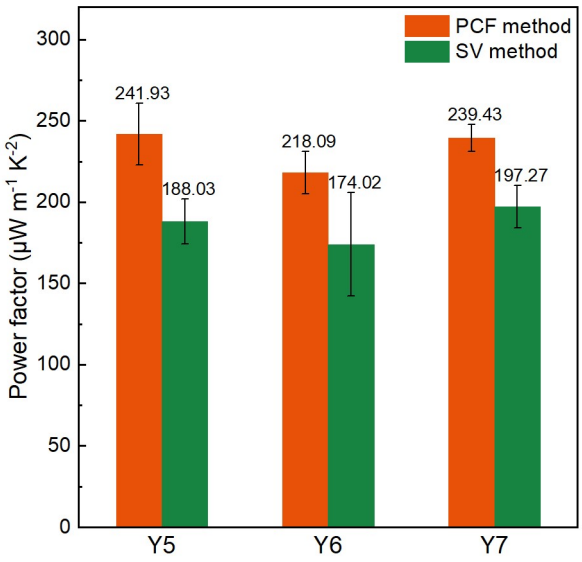

Fig. S3. Comparison of TE performance of Y5, Y6, Y7, and their SWCNT composite films prepared by two methods (orange: PCF, green: SV; the OSM loadings are all 5 wt%).

Table S3. Summary of thermoelectric properties of OSM (5%)/SWCNT composite films prepared by PCF method (OSMs are some classical organic small molecules, and their molecular structures are shown in Fig. S4)

Material	σ (S cm^{-1})	S (μV K^{-1})	PF (μW m^{-1} K^{-2})
Y5/SWCNT	818.91	54.33	241.93 ± 19.06
Y6/SWCNT	656.02	57.53	218.09 ± 10.59
Y7/SWCNT	795.77	55.01	239.43 ± 6.80
ITIC/SWCNT	554.12	57.37	182.44 ± 8.09
ITIC-4F/SWCNT	617.52	58.48	211.22 ± 6.24
ITTC/SWCNT	590.23	58.83	204.19 ± 4.25
IDIC/SWCNT	477.04	59.03	166.35 ± 8.89
IDIC-4F/SWCNT	722.70	56.09	227.42 ± 9.75
IDTPC/SWCNT	415.30	58.96	144.35 ± 5.70

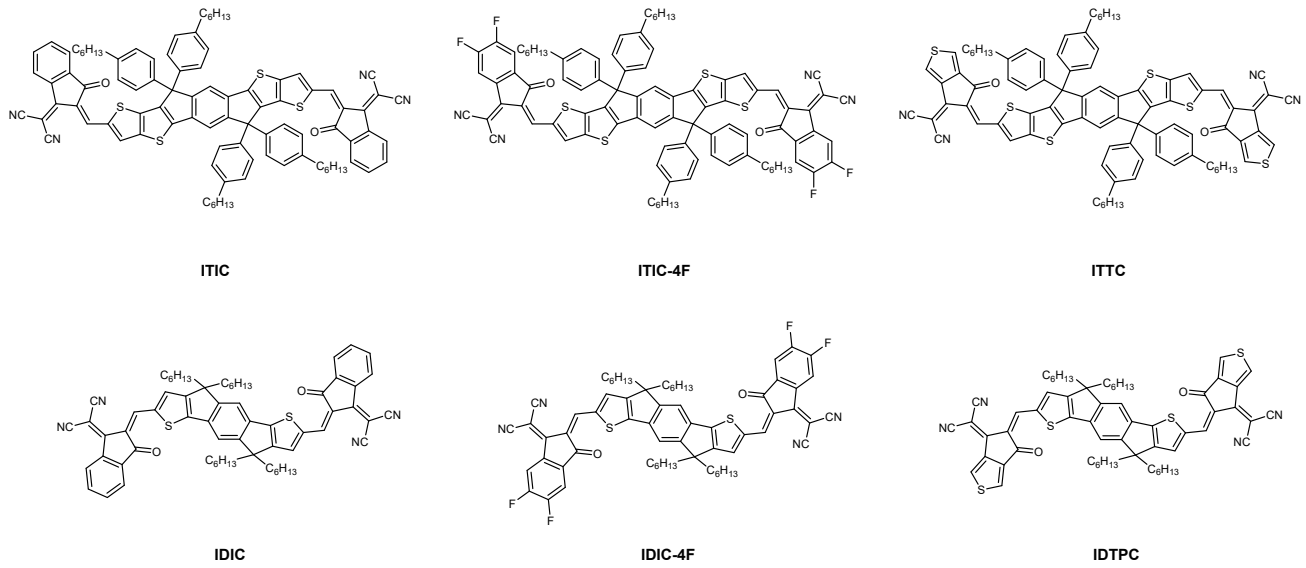

Fig. S4. Part of the molecular structures in Table S3.

Using the UPS spectrum to calculate the work function of the material.

UPS spectra of the secondary electron cutoffs. The cutoff binding energy (E_{cutoff}) and valence band-edge binding energy (E_{VBM}) were obtained from the UPS spectra of the secondary electron cutoffs, and the work function was obtained by subtracting the E_{cutoff} and E_{VBM} from the excitation energy (hv). Taking the original SWCNTs as an example, the W_F were calculated by:

$$W_F = hv - (E_{cutoff} - E_{VBM})$$

$$W_F = 21.22 - (16.03 - (-0.73)) = 4.46 \text{ eV}$$

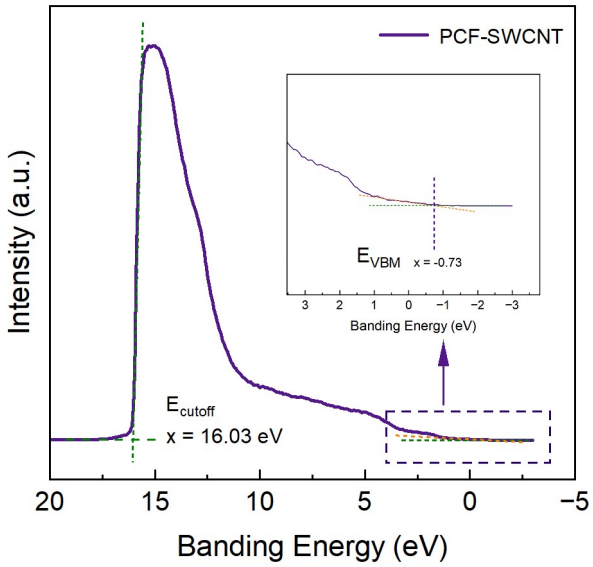

Fig. S5. The secondary electron cutoffs UPS spectrum of the PCF-SWCNT.

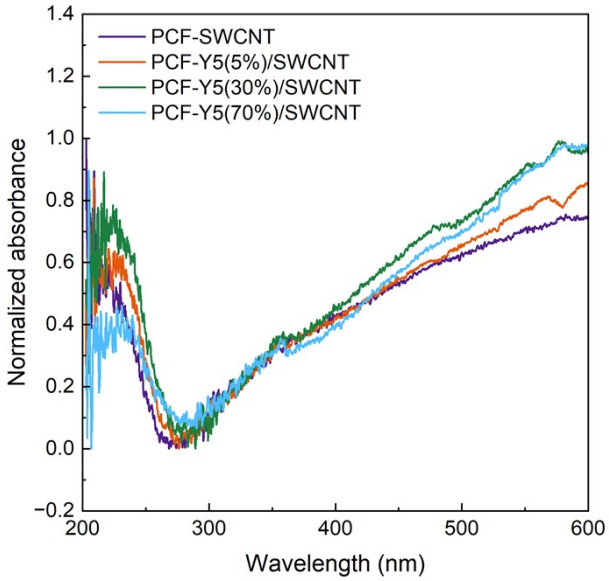

Fig. S6. UV−vis−NIR absorption spectra of PCF-Y5/SWCNT composite films with different Y5 loadings.

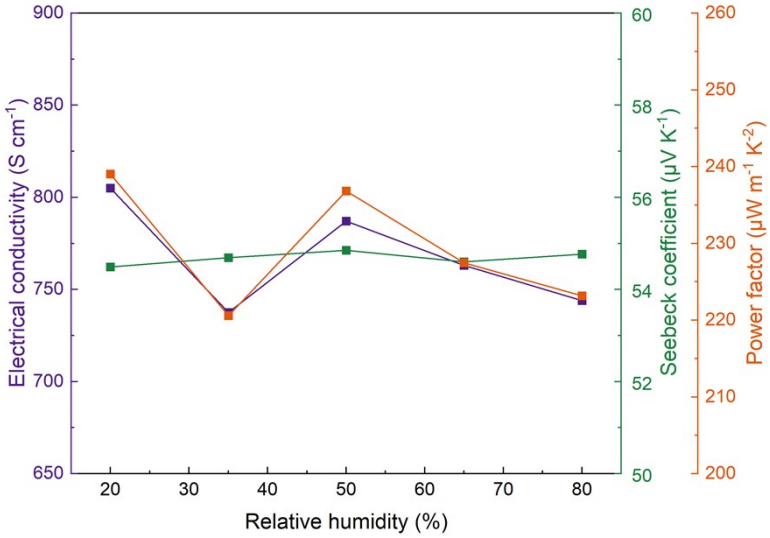

Fig. S7. TE performance of PCF-Y5(5%)/SWCNT composite film at varying relative humidities.

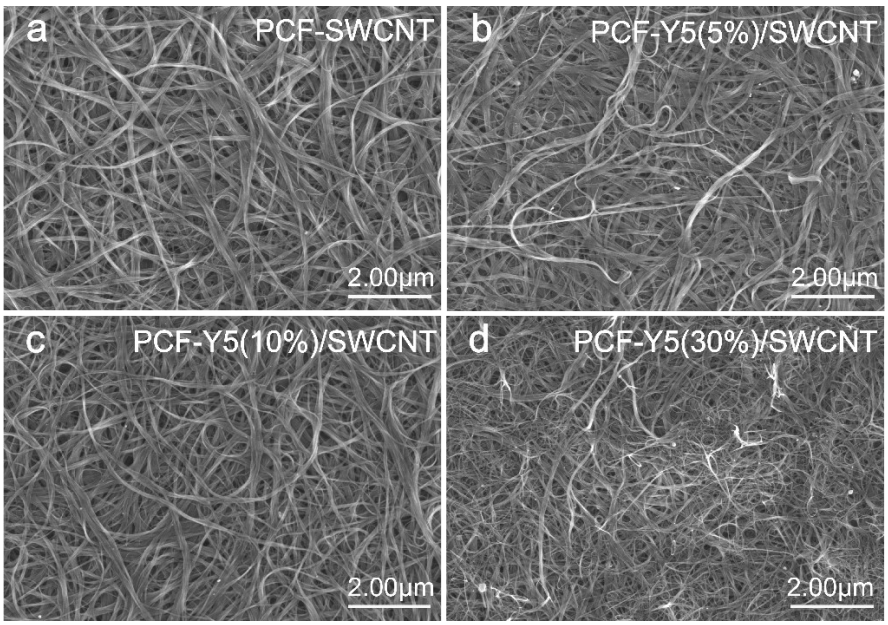

Fig. S8. SEM images of PCF-Y5/SWCNT composite films with different Y5 loading.

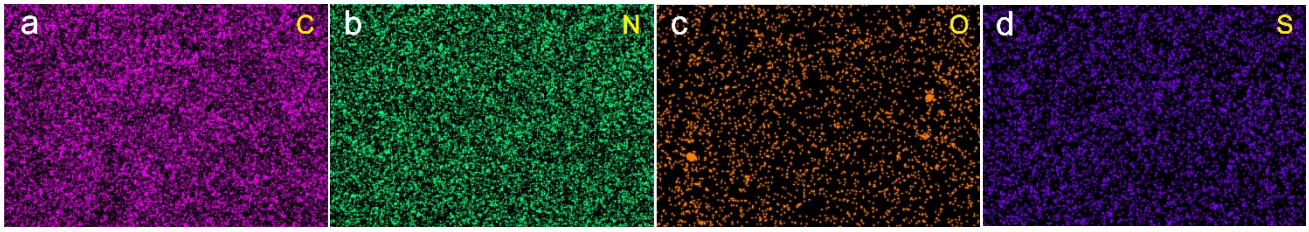

Fig. S9. EDS mappings of PCF-Y5(5%)/SWCNT composite film.

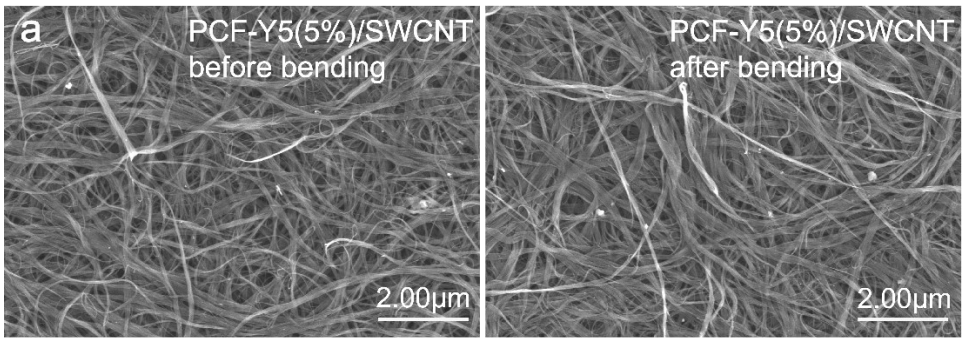

Fig. S10. TEM images of PCF-Y5(5%)/SWCNT composite film before and after bending.

Table S4 The performance of thermoelectric generators (TEGs) based on OSM/SWCNT composites.

Materials	n^a	Voltage (mV)	Power (μW)	Δ*T* (K)	Ref.
C8BTBT–F4TCNQ/SWCNT	5	13.1	0.34	38	22
SWCNT/FcMA	5	22.7	0.75	54.1	23
PDI-2T/SWCNT	5	38.2	0.92	60	24
SWCNT/Lys and SWCNT/Asp	5	42.3	4.3	87	25
Spiro-MeOTAD/ SWCNT	-	9.77	0.057	30	26
PCF-Y5/SWCNT	7	3.8	0.025	20	**This work**
PCF-Y5/SWCNT	7	11.7	0.32	60	**This work**

[a] the number of p–n junctions.

Thermal conductivity test

The parallel thermal conductance method originally proposed by Zawilski, Littleton and Tritt[27] was adapted here to measure the in-plane thermal conductivity of the composite films (around 3 mm × 1.5 mm × 80 μm). The sample holder consists of a strain-gauge heater (R = 350 Ohm) and a copper heat sink. A Kapton stripe which has a low thermal conductivity was used to connect the heater and the heat sink (Fig.S11a). The film sample was attached to the sample holder with silver paste (Fig. S11b). Two T-type thermocouples were employed to monitor the temperature at the hot side and the cold side of the sample, respectively. The sample holder was surrounded by a radiation shield to reduce radiation losses. The whole assembly was placed in a vacuum chamber at 10^{-4} Pa. The total thermal conductance C_{Total} of the sample and the sample holder was conducted by applying multiple DC heating currents (I's) to the heater and generating corresponding steady temperature differences (ΔT's) across the sample. Heating power (P) varies linearly with ΔT as denoted by the following equation:

$$P = I^2 R = C_{\text{Total}} \Delta T \qquad (1).$$

C_{Total} was then extracted from linear fit of the $P \sim \Delta T$ plot.

Later, the sample was cut from the middle and the baseline thermal conductance C_{Baseline} of the setup was determined in a similar way:

$$P = I^2 R = C_{\text{Baseline}} \Delta T \qquad (2).$$

The thermal conductivity κ of the sample is obtained from the following equation:

$$\kappa = (C_{\text{Total}} - C_{\text{Baseline}}) L/A \qquad (3)$$

where L and A are length and cross-sectional area of the sample, respectively.

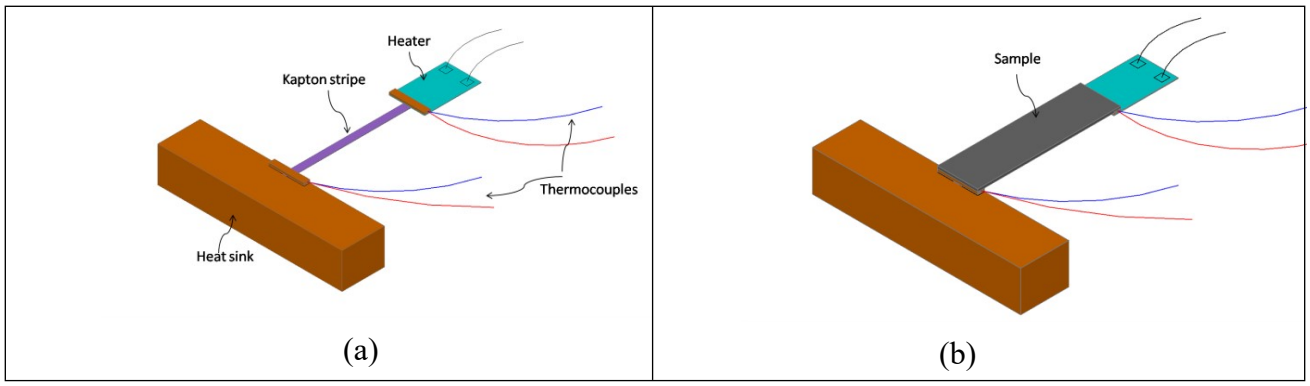

Fig. S11. (a) Configuration of the sample holder for measuring in-plane thermal conductivity; (b) The sample holder mounted with a sample.

NMR spectra

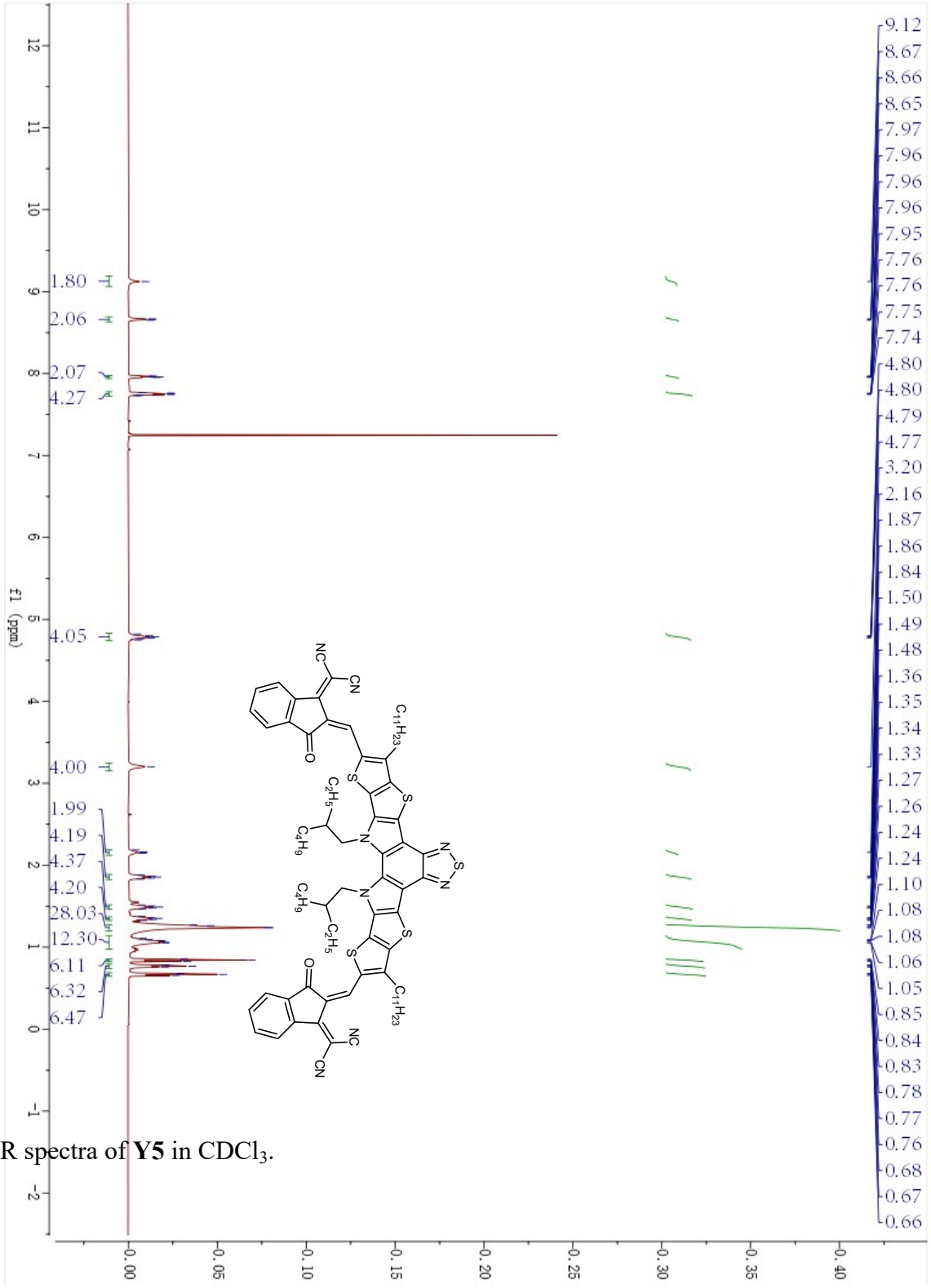

Fig. S12. ^{1}H NMR spectra of **Y5** in $CDCl_3$.

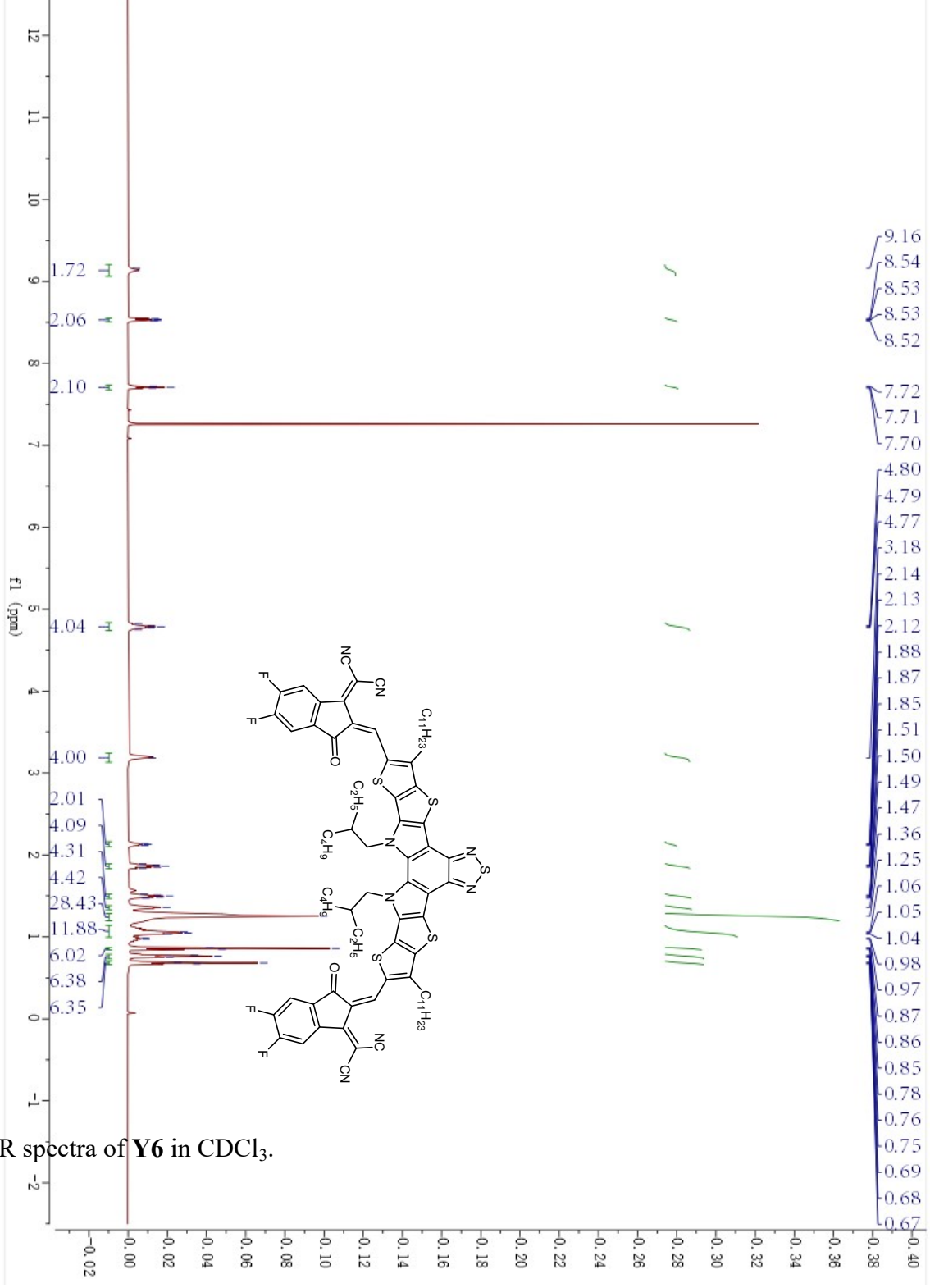

Fig. S13. ^{1}H NMR spectra of **Y6** in $CDCl_3$.

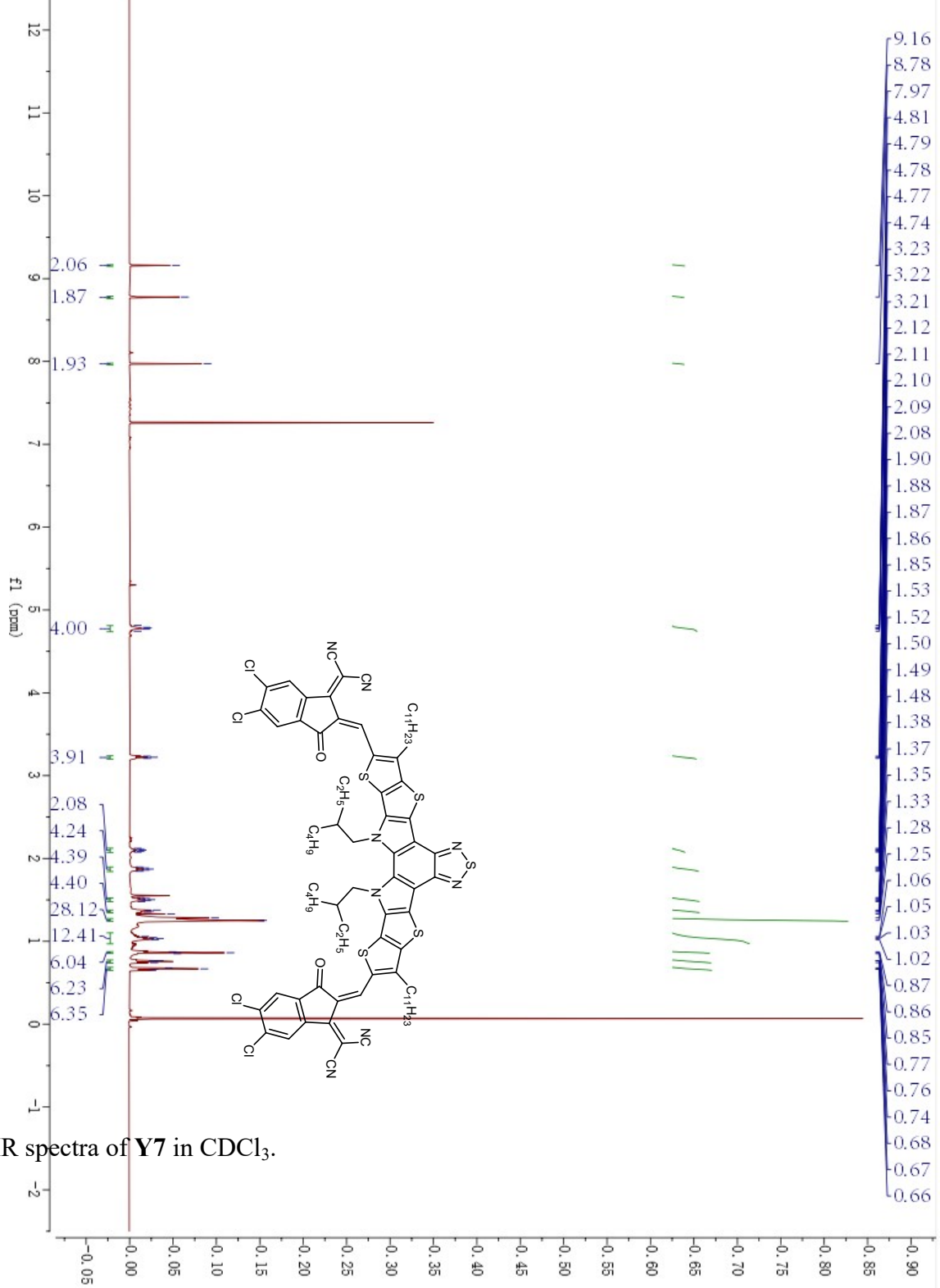

Fig. S14. ^{1}H NMR spectra of **Y7** in $CDCl_3$.

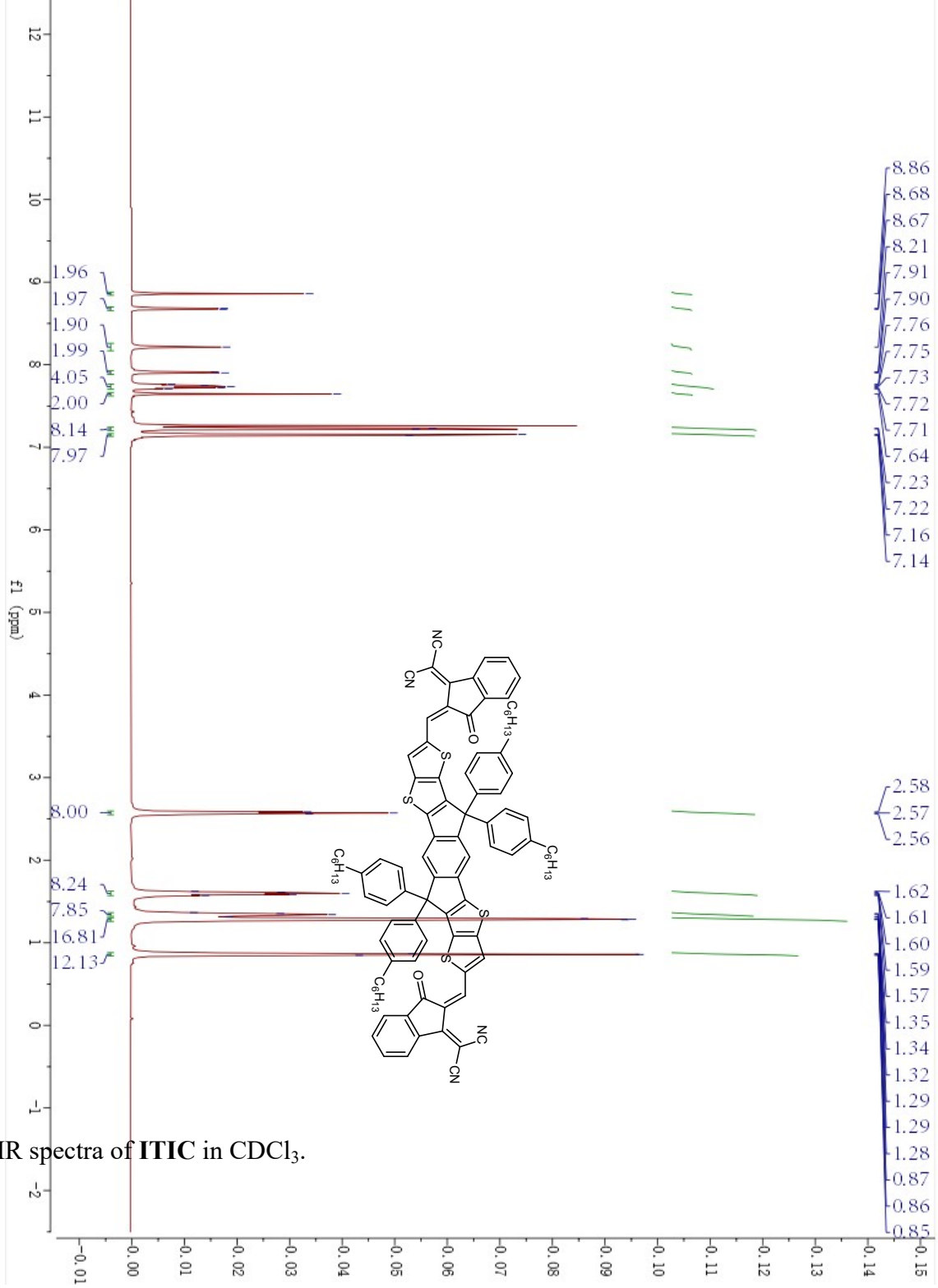

Fig. S15. ^{1}H NMR spectra of **ITIC** in $CDCl_3$.

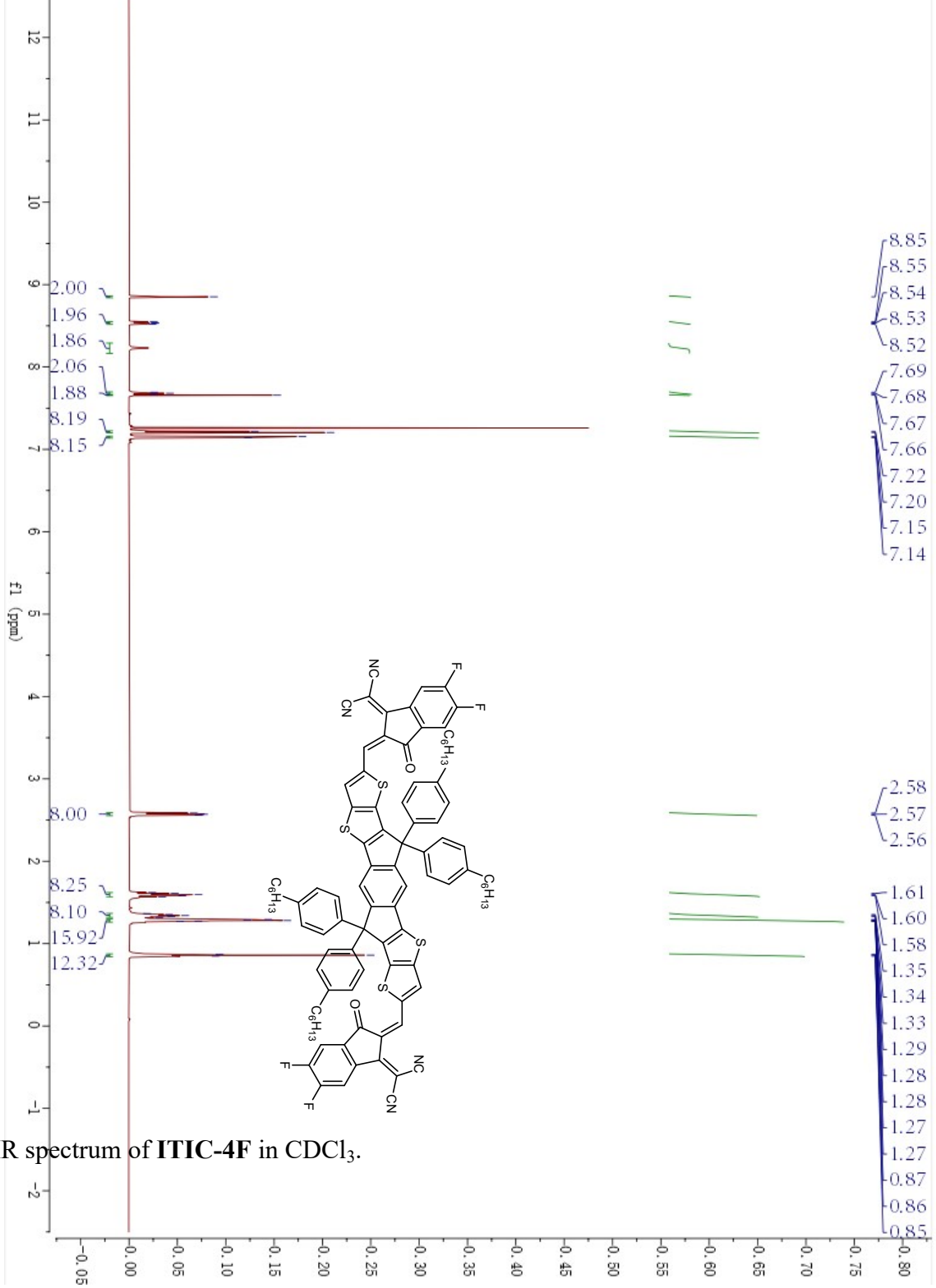

Fig. S16. ^{1}H NMR spectrum of **ITIC-4F** in $CDCl_3$.

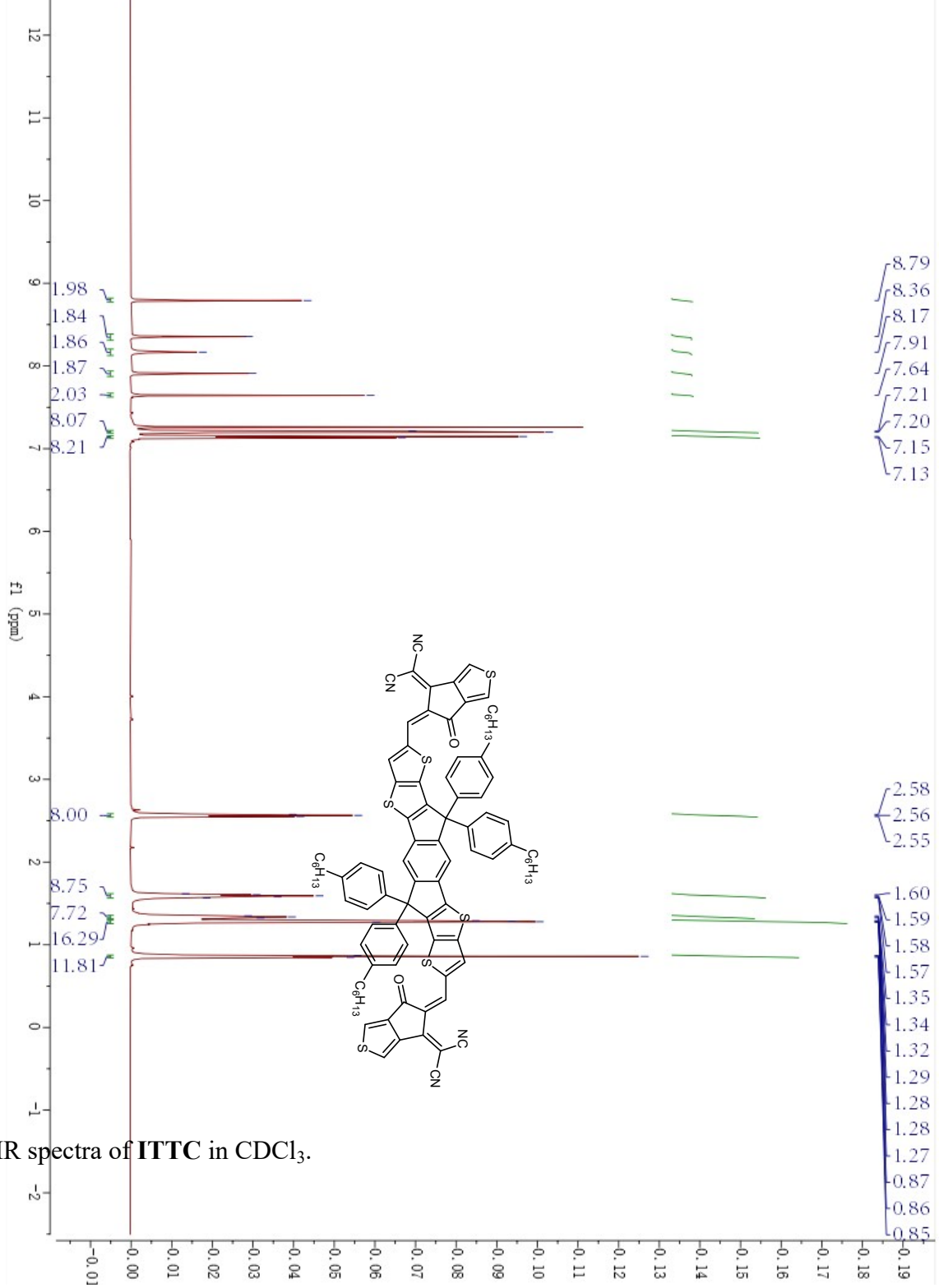

Fig. S17. ^{1}H NMR spectra of **ITTC** in $CDCl_3$.

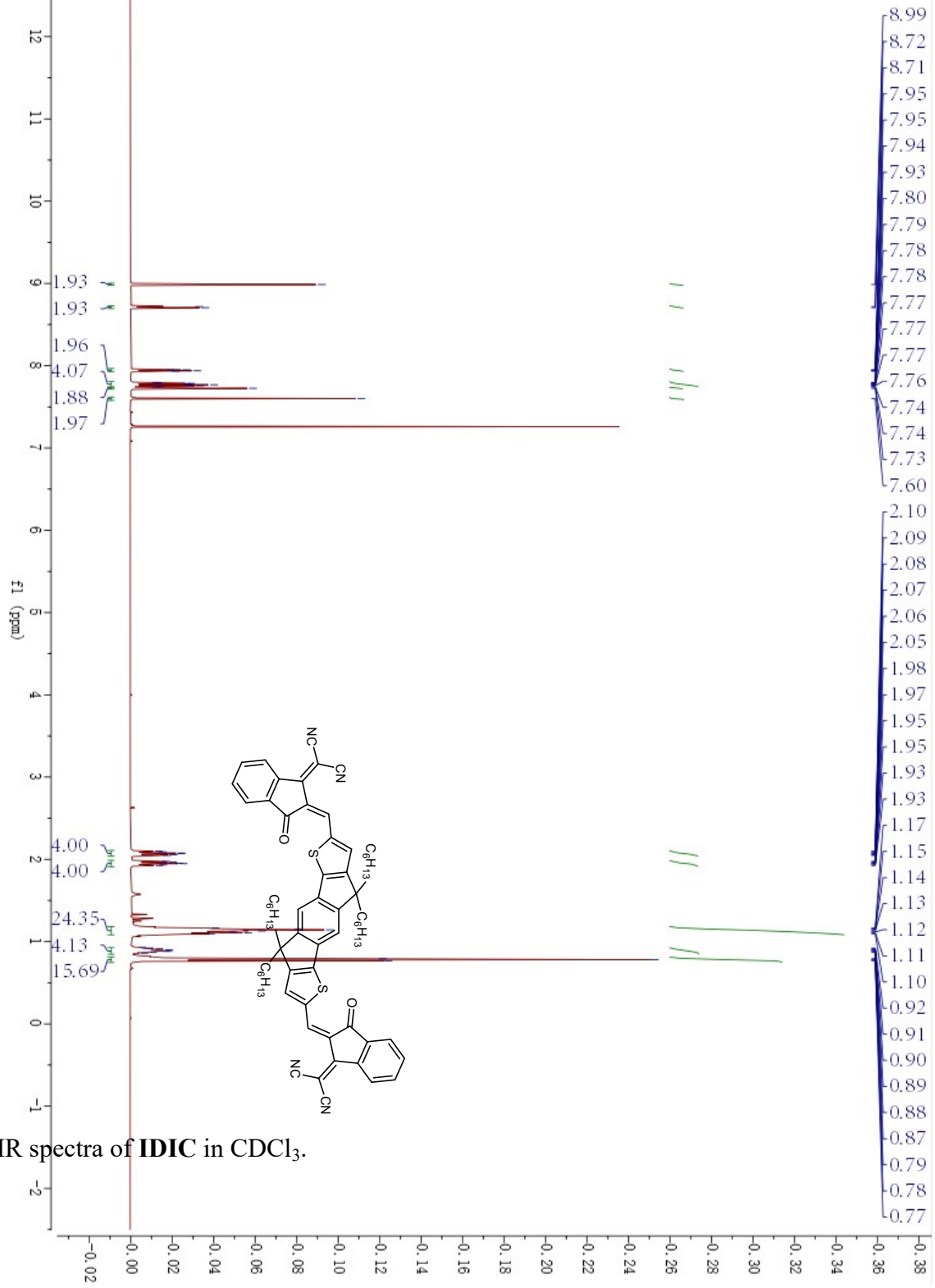

Fig. S18. ^{1}H NMR spectra of **IDIC** in $CDCl_3$.

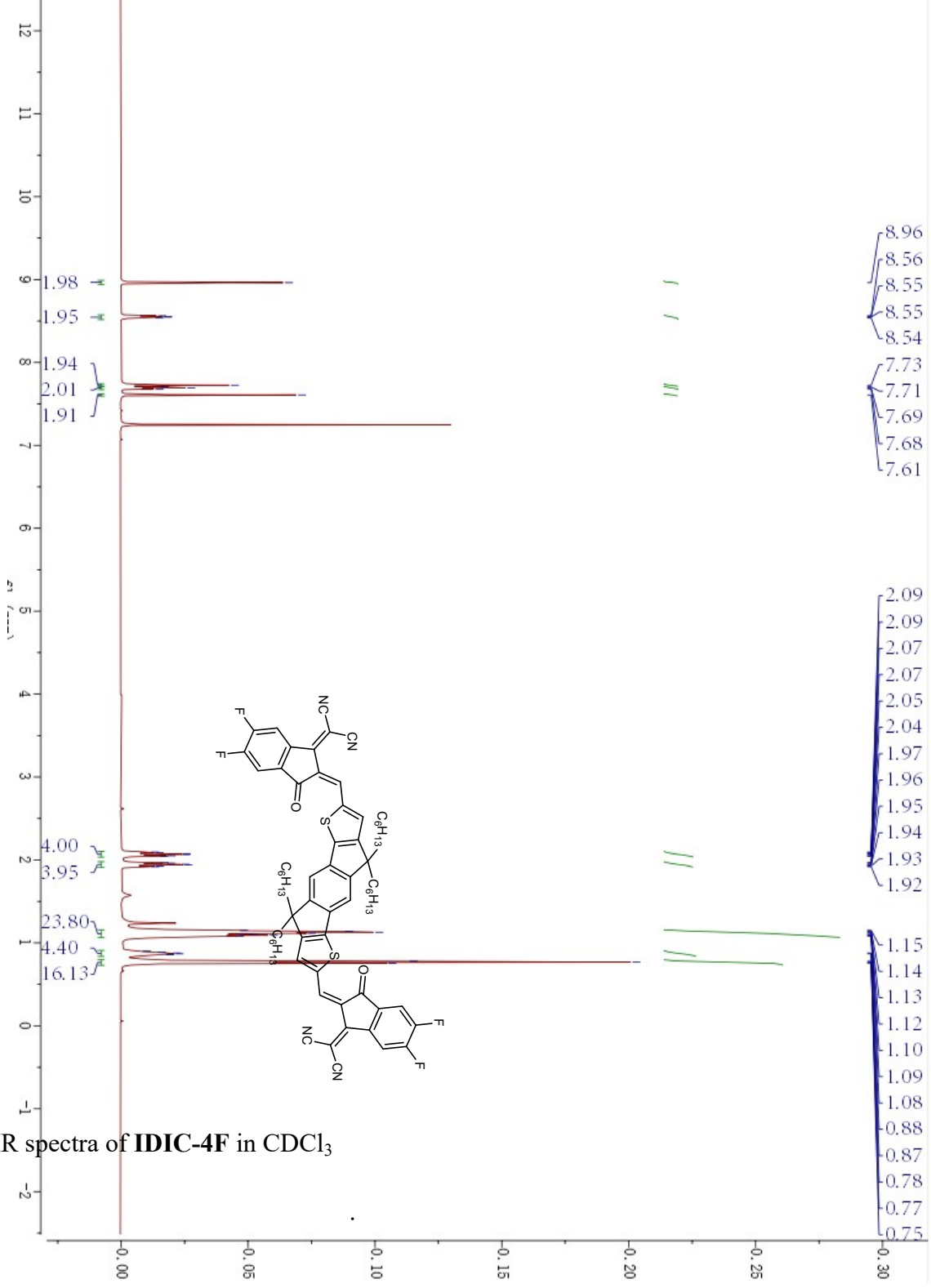

Fig. S19. ^{1}H NMR spectra of **IDIC-4F** in $CDCl_3$

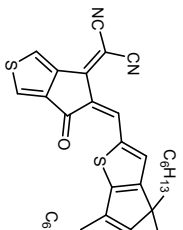

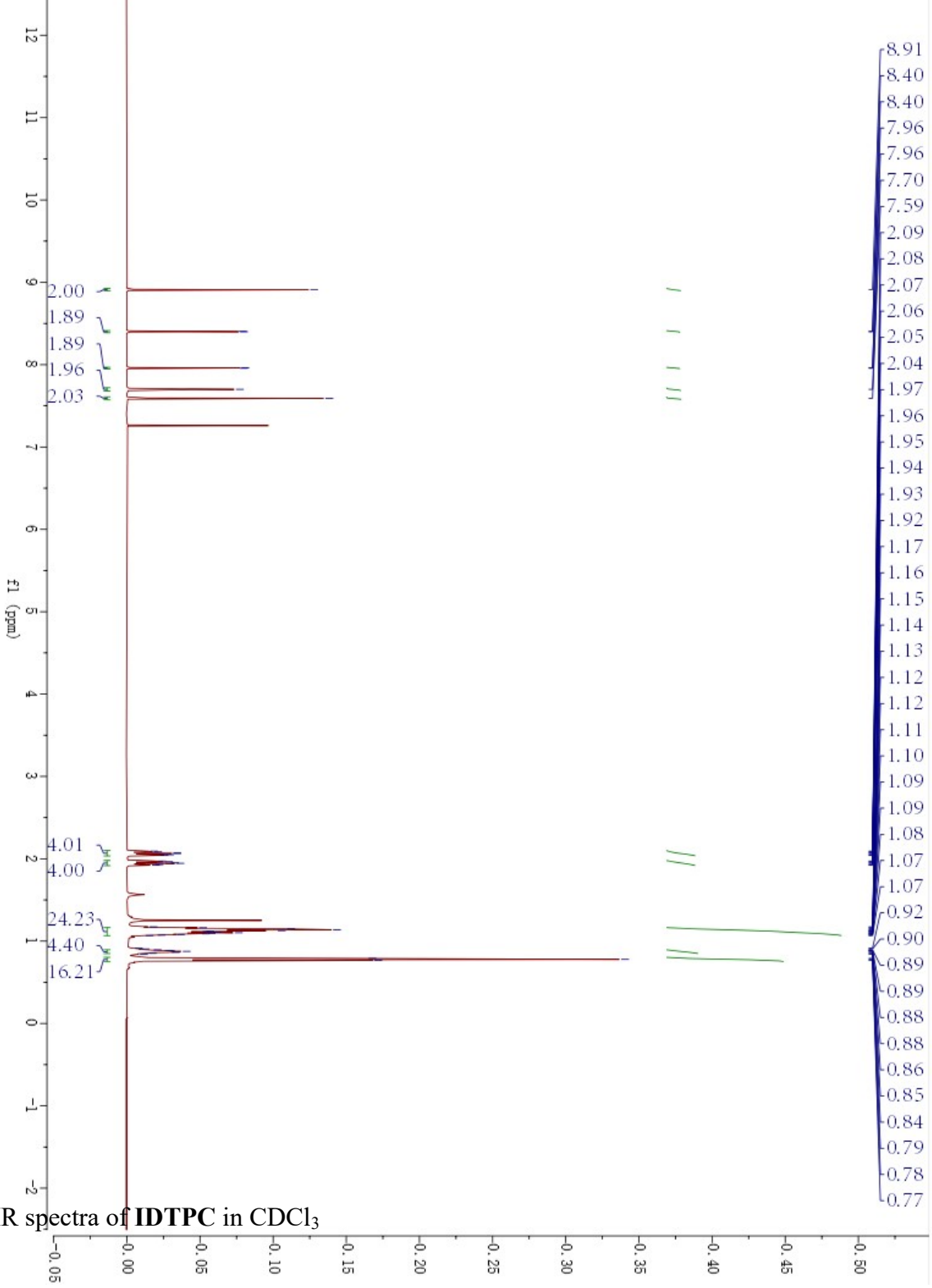

Fig. S20. ^{1}H NMR spectra of **IDTPC** in $CDCl_3$

References

1. Y. Nonoguchi, S. Sudo, A. Tani, T. Murayama, Y. Nishiyama, R. M. Uda and T. Kawai, *Chem Commun*, 2017, **53**, 10259-10262.
2. C. Gao, Y. Liu, Y. Gao, Y. Zhou, X. Zhou, X. Yin, C. Pan, C. Yang, H. Wang, G. Chen and L. Wang, *J Mater Chem A*, 2018, **6**, 20161-20169.
3. F. Liu, X. Zhou, C. Pan and L. Wang, *J Power Sources*, 2019, **412**, 153-159.
4. Y. Zhou, Y. Liu, X. Zhou, Y. Gao, C. Gao and L. Wang, *J Power Sources*, 2019, **423**, 152-158.
5. N. Feng, C. Gao, C.-Y. Guo and G. Chen, *ACS Appl Mater Interfaces*, 2018, **10**, 5603-5608.
6. X. Li, Z. Yu, H. Zhou, F. Yang, F. Zhong, X. Mao, B. Li, H. Xin, C. Gao and L. Wang, *ACS Sustainable Chem Eng*, 2021, **9**, 1891-1898.
7. B. Li, Y. Mao, X. Mao, Y. Liu, X. Li, Y. Zhou, S. Wang, F. Yang, C. Gao and L. Wang, *ACS Appl Energy Mater*, 2020, **3**, 11947-11955.
8. T.-h. Kim and J.-I. Hong, *ACS Appl Mater Interfaces*, 2022, **14**, 55627-55635.
9. P. Li, H. Guo and H. Xu, *J Mater Sci*, 2022, **57**, 18524-18534.
10. S. Yin, X. Wu, R. Wang and C. Y. Guo, *Macromol Mater Eng*, 2022, **307**.
11. D. Zheng, J. Zhang, S. Sun, J. Liang, Y. Li, J. Luo and D. Liu, *ACS Appl Electron Mater*, 2024, **6**, 4754-4763.
12. S. Wei, L. Liu, X. Huang, Y. Zhang, F. Liu, L. Deng, E. Bilotti and G. Chen, *ACS Appl Mater Interfaces*, 2022, **14**, 5973-5982.
13. G. Li, C. Chen, Z. Liu, Q. Sun, L. Liang, C. Du and G. Chen, *Mater Horiz*, 2024, **11**, 1679-1688.
14. X. Wu, S. Yin and C.-Y. Guo, *ACS Appl Mater Interfaces*, 2022, **14**, 32056-32065.
15. H. Fu, J. Yao, M. Zhang, L. Xue, Q. Zhou, S. Li, M. Lei, L. Meng, Z.-G. Zhang and Y. Li, *Nat Commun*, 2022, **13**, 31389.
16. R. Takahashi, T. Seo, K. Kubota and H. Ito, *ACS Catal*, 2021, **11**, 14803-14810.
17. R. Takahashi, A. Hu, P. Gao, Y. Gao, Y. Pang, T. Seo, J. Jiang, S. Maeda, H. Takaya, K. Kubota and H. Ito, *Nat Commun*, 2021, **12**.
18. T. Seo, K. Kubota and H. Ito, *J Am Chem Soc*, 2020, **142**, 9884-9889.
19. K. Kubota, T. Seo, K. Koide, Y. Hasegawa and H. Ito, *Nat Commun*, 2019, **10**.
20. K. Kubota, Y. Pang, A. Miura and H. Ito, *Science*, 2019, **366**, 1500-1504.
21. J. Yuan, Y. Zhang, L. Zhou, C. Zhang, T. K. Lau, G. Zhang, X. Lu, H. L. Yip, S. K. So, S. Beaupré, M. Mainville, P. A. Johnson, M. Leclerc, H. Chen, H. Peng, Y. Li and Y. Zou, *Adv Mater*, 2019, **31**, 1807577.
22. S. Qin, J. Tan, J. Qin, J. Luo, J. Jin, S. Huang, L. Wang and D. Liu, *Adv Electron Mater*, 2021, **7**, 2100557.
23. X. Nie, X. Mao, X. Li, J. Wu, Y. Liu, B. Li, L. Xiang, C. Gao, Y. Xie and L. Wang, *Chem Eng J*, 2021, **421**, 129718.
24. J. Liang, S. Sun, S. Huang, J. Jin, D. Zheng, J. Luo and D. Liu, *Mater Today Commun*, 2023, **35**, 106317.
25. G. Cao, X. Nie, Z. Ren, Y. Wu, J. Yang, J. Wei, J. Wu, L. Wang and C. Gao, *ACS Sustainable Chem Eng*, 2022, **10**, 12009-12015.

26. K. Zhu, Z. Hu and G. Chen, *Compos Commun*, 2022, **32**, 101166.
27. B. M. Zawilski, R. T. Littleton and T. M. Tritt, *Rev Sci Instrum*, 2001, **72**, 1770-1774.